Proceedings of the ASME 2010 3rd Joint US-European Fluids Engineering Summer Meeting and 8th International Conference on Nanochannels, Microchannels, and Minichannels
FEDSM-ICNMM2010
August 1-5, 2010, Montreal, Canada

FEDSM-ICNMM2010-31030

THE EFFECT OF MACH NUMBER AND ASPECT RATIO ON THE INTERFACIAL CHARACTERISTICS OF A SUBMERGED RECTANGULAR GAS JET

Chris Weiland
Virginia Tech Department of Mechanical Engineering

Pavlos Vlachos
Virginia Tech Department of Mechanical Engineering

ABSTRACT

Gas jets formed by rectangular nozzles submerged in water were studied using a non-invasive photographic technique which allowed simultaneous measurements of the entire interface. Three aspect ratios were considered corresponding to 2, 10, and 20 with all nozzles sharing a common width. As far as the authors know this study represents the first time the effects of aspect ratio and Mach number on a submerged gas jet have been studied. The results indicate aspect ratio and Mach number play a large role in dictating both the unsteadiness of the interface and the penetration of the gas jet into the surrounding liquid medium. The jet pinch-off is shown to have a logarithmic decay with increasing Mach number and when appropriately scaled by the total viewing length and a geometric length scale (L_Q) is relatively constant across all aspect ratio nozzles. The location of pinch-off is also a function of aspect ratio, with the subsonic aspect ratio 2 nozzles showing maximum pinch-off at $y/L_Q \approx$ 23-26 while sonic and supersonic Mach numbers have peaks over the range $y/L_Q \approx$ 11-14. The AR 10 and 20 nozzles show no dependence on Mach number with the maximum number of pinch-off events observed over the interval $y/L_Q \approx$ 3-5. Jet spreading which is indicative of liquid entrainment is also shown to increase with Mach number and aspect ratio. The jet penetration also increases with increasing Mach number and aspect ratio. The spatial instability growth rate was deduced from the downstream evolution of the interfacial unsteadiness and it is shown that the nozzle with aspect ratio of 2 follows a different trend than the aspect ratio 10 and 20 nozzles, suggesting a fundamentally different mechanism dominates the stability of large aspect ratio rectangular gas jets.

INTRODUCTION

While the structure and stability of single phase jets have been studied extensively for quite some time, two-phase flow systems formed by a submerged compressible gas jet have received very little attention. The metallurgical industry uses submerged round gas jets for liquid metal stirring and gas-metal reactions as the gas jet enhances mixing efficiency through the high surface to volume ratio of the bubbly mixture [[1]; [2]]. Since the focus of submerged gas injection in most cases is usually on enhancing mixing and mass transfer, rectangular jets are excellent for achieving these goals. Single phase rectangular jets naturally exhibit higher mixing at the interface than circular jets when the aspect ratio increases past approximately 10 [3]. Although most studies have focused on round [[4]; [5]] or planar [6] gas jets injected into quiescent liquid, the present study focuses on the injection of a rectangular gas jet exhausted into quiescent liquid. In particular, we seek to characterize the effects of aspect ratio and Mach number on the interfacial structure formed by the two-phase system.

While gas jets submerged in liquid are not understood very well, single phase plane and rectangular jets are extensively analyzed [[7]; [8]]. Planar jets include end-walls at either end of the nozzle span to limit three-dimensional effects while rectangular jets omit the end-walls. Here we review both planar and rectangular jets in order to illustrate some of the physics common to both configurations.

Of particular interest to the present study is the existence of ordered structure in the plane jet. The experiments of Antonia et al [9] support the existence of counter-rotating spanwise structures through space-time correlations of point measurements in the planar jet. Near the jet exit prior to merging of the shear layers, these structures are symmetric about the centerline. The structures are asymmetric after the shear layers merge. Gordeyev and Thomas [[10]; [11]] provided an exhaustive analysis of the similarity region of a turbulent planar jet and directly observed the asymmetry of the large scale structures. They note that these structures interact with one another, which could explain the "jet flapping" commonly observed in plane jets. The jet was acoustically

excited above and below the long dimension of the nozzle orifice at the fundamental frequency while varying the phase between the two acoustic excitation sources. They found that many aspects of the jet such as spreading rates, velocity fluctuations, and their spectral distributions can be effectively controlled through artificial excitation, which is a further manifestation of the importance of the shear layer merger on the bulk jet properties.

Single phase rectangular jets have also been studied although with much less frequency than planar or axisymmetric jets. Rectangular jets, with no end-plate to limit three-dimensional effects near the nozzle, have been shown to have three-dimensional effects and provide a convenient flow field for studying three-dimensional effects in shear layers [[12]; [13]]. Hot-wire measurements by Krothapalli et al [14] and the work of Sforza et al [12] indicate three regions in the development of a rectangular jet, namely the potential core (initial) region, a two-dimensional (characteristic) region, and an axisymmetric (fully developed) region; the latter two regions are characterized by their velocity profiles and decay rates, which resemble either two-dimensional planar or axisymmetric velocity profiles respectively. The results of Krothapalli et al [14] and others suggest that the two-dimensional region begins to develop when the shear layers from the small nozzle dimension merge, and the axisymmetric character develops when the shear layers from the large nozzle dimension merge. In the axisymmetric region all memory of the original nozzle configuration is lost. Sforza et al [12] identify a fourth region in which the flow is fully axisymmetric far downstream of the orifice.

For the case of rectangular jets as opposed to planar jets the path to a fully axisymmetric flow is enhanced due to mixing at the corners of the rectangular nozzle, which introduce sharp gradients and tend to smear rapidly and enhance mixing. Tam and Thies [15] derived the equations of stability for a rectangular jet using a vortex sheet model and numerically showed four linearly independent families of instability waves. The first and third are due to the nozzle corners, and as such tend to dampen out as the jet mixes and becomes more axisymmetric. Thus the literature contains two competing explanations for why the rectangular jet transitions towards an axisymmetric configuration: the sharp gradients located at the nozzle corners and the merging of the jet shear layers. In planar jets, it is commonly accepted that the merger of the shear layers (from the small nozzle dimension) play a role in the mean jet characteristics, such as potential core length, although some evidence suggests that aspect ratio may play a role as well [7].

The effect of aspect ratio on mean flow characteristics in rectangular jets has been studied in some detail. Common to large (>5) aspect ratio rectangular jets is the saddle-shaped mean streamwise velocity profile [[14]; [12]; [16]]. Quinn [17] studied two rectangular nozzles having aspect ratios of 2 and 10 and confirmed the presence of the saddle-shaped mean streamwise velocity profile for aspect ratio 10 and its failure to exist for an aspect ratio 2 nozzle. Tsuchiya and Horikoshi [18] studied small aspect ratio rectangular jets as well, with nozzles having aspect ratios less than 5. They found a large difference in the turbulence intensity as a function of aspect ratio. Krothapalli et al [14] also reported the effects of aspect ratio on the development of single phase rectangular jets and note that the downstream distance where the velocity profile follows similarity seems to depend on aspect ratio, mainly due to merging of the shear layers located in the plane of the long nozzle dimension. Using hot-wire anemometer measurements Sfeir [16] confirmed the importance of aspect ratio on velocity decay and more importantly, showed the departure from two-dimensional effects which are related to the nozzle aspect ratio.

The injection of gas into liquid introduces an additional level of complexity in the jet character, which is marked by unsteadiness and pulsating of the phase interface. The submerged jet can even rupture into bubbles which rise independently, a phenomenon known as pinch-off. When pinch-off occurs near the orifice damage to the submerged injector can occur [19]. To prevent damage to the injector it is common for submerged jets in both planar and round configurations to operate with a sonic (convergent) nozzle. Loth and Faeth [6] reported the internal structure of vertical underexpanded planar nozzles. Underexpansion ratios as high as 4 were tested and as a result pressure measurements taken inside the gas jet showed the presence of a shock-cell expansion region downstream of the nozzle exit for the first time. Also, void fraction measurements indicated that the half-widths were 2 to 3 times greater than that of single phase plane jets. However their measurements, such as the interface position, are only time averaged quantities. In fact all past measurements of multiphase gas systems known to the authors utilize time averaged quantities to deduce physical mechanisms responsible for the observed behaviors. These analysis methods conflict with what many past studies have shown, namely that the interface is dynamic and constantly evolving.

The goal of the present experiment is to study the interfacial character of the submerged rectangular gas jet. While the nozzle and flow system were instrumented to provide measurements of the internal nozzle Mach number at the jet exit plane, no measurements of the internal jet structure were taken. In particular, compressibility (Mach 0.4-1.5) and aspect ratio (2, 10, and 20) were varied to ascertain their effects on the jet penetration and interface characteristics, which was measured directly using high speed digital photography. To the authors' knowledge, this study represents the first study of submerged rectangular gas jets and the first time quantitative time-resolved measurements of the interface position have been attempted.

NOMENCLATURE

AR – aspect ratio (l/w)
l – length of nozzle (long dimension)
L_Q – length scale (l)
M – Mach number
P – pressure (Pa)

T – temperature (K)
x – radial position (m)
y – axial position (m)
w – width of nozzle (short dimension)

Subscripts
e – exit conditions
H – hydrostatic conditions
o – stagnation conditions
p – penetration distance

EXPERIMENTAL

The experiments were conducted in the Advanced Experimental Thermofluid Engineering Research Laboratory of the Mechanical Engineering Department at Virginia Tech. The experimental setup is shown in Figure 1 and consists of a clear acrylic tank, an injector assembly, pressure and temperature sensors, a fast acting valve which impulsively switched on the gas injection, and a high speed camera which recorded shadowgraph images of the underwater jet. The tests were controlled by a LabVIEW program which simultaneously triggered the high speed camera (Photron APX-RX), monitored various gas pressures and temperatures, and opened the fast acting valve which delivered gas flow to the injector. This allowed for the establishment of an accurate reference time, and synchronization between the sensors and the recorded images. The test matrix is shown in Table 1 where all properties, such as the Reynolds and Richardson numbers, are calculated based on the initial (orifice exit) properties. Here the Reynolds number uses the nozzle width (short dimension) as the characteristic length scale. The Mach number is calculated for the gas phase only at the exit of the nozzle.

Table 1. Test matrix for all Mach numbers tested. All jets were shot at 0.46m water depth and the properties shown here were calculated for the nozzle exit.

	Mach Number	P_e (Pa x10^5)	P_o (Pa x10^5)	P_e/P_o	P_e/P_H	T_o (K)	Mass Flow (kg/s)	Velocity (m/s)	Reynolds No (x10^4)
AR 2	0.50	1.05	1.13	0.93	1.013	300.2	0.0010	165	1.72
	0.63	1.05	1.17	0.90	1.014	300.6	0.0013	210	2.14
	0.82	1.05	1.27	0.83	1.014	300.7	0.0018	270	2.70
	0.97	1.05	1.51	0.70	1.016	300.8	0.0023	320	3.14
	1.10	1.09	2.28	0.48	1.052	299.9	0.0034	340	3.46
	1.36	1.04	3.07	0.34	1.006	300.1	0.0047	401	4.08
	1.50	1.04	3.71	0.28	1.002	300.8	0.0050	430	4.38
AR 10	0.48	1.03	1.09	0.94	0.989	300.6	0.0040	165	1.64
	0.64	1.03	1.15	0.89	0.99	300.7	0.0055	210	2.16
	0.84	1.04	1.29	0.81	0.999	300.4	0.0078	270	2.76
	1.01	1.06	1.55	0.69	1.025	300.2	0.0105	320	3.24
	1.07	1.09	1.98	0.55	1.047	299.8	0.0125	340	3.40
	1.36	1.04	2.79	0.37	0.999	300.6	0.0176	401	4.10
	1.52	1.04	3.57	0.29	1.003	300.5	0.0201	430	4.42
AR 20	0.47	1.05	1.10	0.95	1.01	300.3	0.0074	165	1.62
	0.60	1.05	1.16	0.91	1.014	300.2	0.0100	210	2.02
	0.80	1.06	1.24	0.85	1.02	300.7	0.0142	270	2.65
	1.00	1.08	1.44	0.75	1.037	300.6	0.0192	320	3.20
	1.13	1.07	1.68	0.64	1.031	300.9	0.0207	340	3.56
	1.30	1.05	2.22	0.47	1.009	299.8	0.0262	401	3.96
	1.57	1.03	3.27	0.93	0.995	299.6	0.0343	430	4.52

The injector was rigidly held upright in an acrylic tank using a steel bracket bolted to the injector as shown in Figure 1. The injectors were submerged in an acrylic tank at a constant depth of 0.46 m with a wave breaker constructed from 3 layers of perforated sheet to limit surface waves and provide a constant hydrodynamic pressure, which was calculated using a Druck PTX-7217 barometric load cell (range: 79–120 kPa absolute, 0.1% full scale accuracy) to measure the atmospheric pressure and a known and closely controlled water depth. Although past researchers have shown that wave dampers do little to change the flow characteristics [[4]; [20]], the wave damper has the added benefit of forcing the ambient waters to reach a quiescent conditions more quickly after a test.

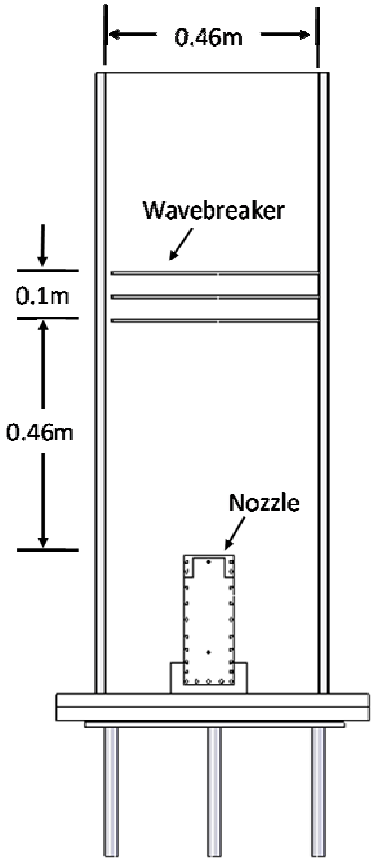

Figure 1. View of the injector inside the acrylic tank. Perforated sheets helped to control surface disturbances. A steel angle bracket was bolted to the injector to secure it upright.

Three injectors having aspect ratios of 2, 10, and 20 were studied with a common width (*w*) of 1.5mm (0.0625 inches) with three lengths (l). The nozzles were cut from Acrylic sheet using a Universal Laser CNC laser cutter to dimensions specified in CAD drawings. The nozzle dimensions were measured to ensure accuracy. For each aspect ratio four nozzles were CNC laser cut: one nozzle for the subsonic (Mach 0.5, 0.6, and 0.8) and sonic test cases and one for each supersonic Mach number (1.2, 1.3, and 1.5). Three trials of each test case were recorded. The nozzles were sandwiched between two aluminum plates as shown in Figure 2 and held together with a system of bolts around its perimeter. This unit consisting of the two aluminum side plates and the nozzle insert will hereafter be referred to as the injector. The left picture of Figure 2 illustrates the aluminum sides which sandwich the interchangeable nozzle insert, shown as the right picture. Vacuum grease placed between the nozzle insert and the aluminum sides formed a high pressure seal prohibiting gas leakage from all sides. Air was delivered via two gas injection ports and the stagnation pressure was measured in the gas inlet chamber.

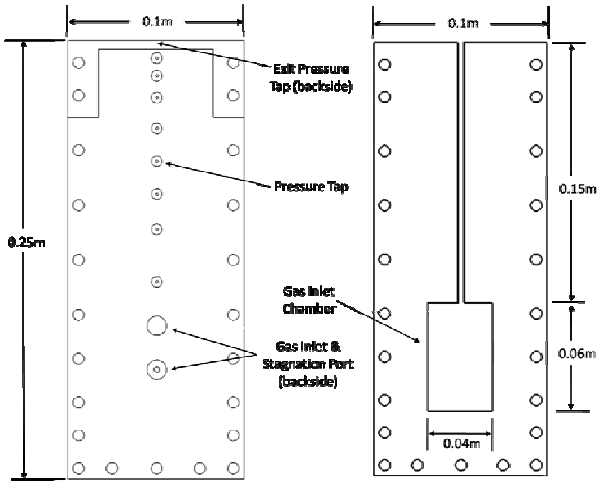

Figure 2. The injector is composed of three pieces, the two outer aluminum side plates and the nozzle insert. Picture on left shows outer aluminum piece while the right picture shows the subsonic/sonic aspect ratio 2 nozzle insert.

Image Processing Techniques

A schematic illustrating the instrumentation and control system is shown in Figure 3. The system was designed to deliver a constant mass flow to the injector. A pressure reservoir ($0.23m^3$ volume) was used in conjunction with a gas pressure regulator (Generant model 2GDR-1000B-V-B) that was insensitive to backpressure changes (1.7 kPa output change in flow pressure given 0.69 MPa input change) in reservoir pressure. The pressure downstream of the gas regulator was monitored to ensure a constant delivery pressure. Prior to each test the pressure reservoir was charged from an external gas source until the maximum pressure was attained. The manual valve was then closed to prohibit any line pressure spikes from interfering with the injector gas flow. During each test, the change in the vessel pressure and temperature was monitored to calculate the mass flow rate delivered to the injector using the ideal gas equation. In all cases dried air was used as the working fluid and untreated tap water was used as the quiescent fluid.

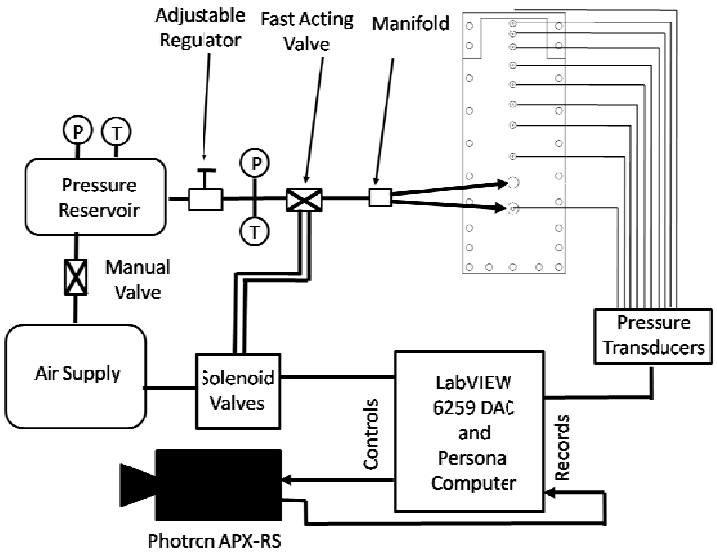

Figure 3. Schematic of the instrumentation and control system. Gas flow was started and stopped using a fast acting pneumatic valve controlled by LabVIEW software, which also triggered all instrumentation.

The system was controlled by LabVIEW software in conjunction with a National Instruments 6259 16-bit DAC. Upon running the software, a low voltage signal is transmitted to both the Photron camera and a solenoid valve which causes the camera to begin recording and the fast acting valve (W.E. Anderson ¾" NPT, model ABV1DA103) to open simultaneously. The fasting acting valve has an opening time of about 0.03s. Not shown in Figure 3 are 10 Clippard (model EV-2-24) solenoid valves controlled by the DAC which deliver compressed gas to the pressure lines while the injector is off. The compressed gas prohibited water intrusion into the pressure lines.

Pressure measurements were taken at a 1 kHz sampling rate with Druck 7217-PTX transducers with an accuracy of 2% full scale. Several ranges of transducers were used to measure signals of different expected pressure ranges in an effort to minimize errors. Transducers with a range of 0-0.35 MPa were used to measure pressures at and downstream of the nozzle throat while upstream of the nozzle throat transducers with a range of 0-0.70 MPa were used. Temperature measurements were made at the pressure reservoir and just downstream of the adjustable pressure regulator using type K thermocouples with an Omega thermocouple to analog converter (model SMCJ-K) for a total accuracy of +/- 3 deg C. The Mach number was calculated using the isentropic law relating pressure and Mach number. Due to propagation of uncertainties in the pressure measurements, the error in the Mach number measurements at the nozzle exit was approximately 1% (Mach 1.8) - 7% (Mach 0.4). Considerable effort went into ensuring, in the case of the sonic and supersonic nozzles, that the gas jets were perfectly expanded by monitoring the exit pressure and the known hydrostatic pressure.

Photographic Measurements and Edge Detection

A Photron FASTCAM APS-RX in conjunction with a Canon VX-16 telephoto lens was used to digitally record shadowgraph images of the test section at 1 kHz sampling rate for 9 seconds. The typical magnification used in the tests was approximately 388 μm/pixel. Eight 250W halogen lamps evenly distributed over the test section were arranged behind a white sheet to distribute light evenly over the test section. Acquired images were processed in MATLAB to detect the gas jet boundary in time. As the shadowgraph produces a projection of the gas jet onto a two-dimensional image, no three-dimensional information is collected. The jet boundary is computed using the steps shown in Figure 4. First the image is binarized based on a threshold pixel intensity to capture the gas phase and a 7x7 pixel median filter is applied to smooth any irregularities such as bubbles fractured from the jet. Next a circular disk morphological element was applied to the binarized image and after dilation and erosion the perimeter of the resulting structure was identified. As shown in Figure 4 the detected boundary agrees quite well with the experimental image. To ensure the jet reached steady-state behavior the jet boundaries were tracked ½ second after the gas jet was initiated. All jets had reached the free surface prior to analysis. The computed edges were tracked and their positions recorded for all times which allowed not only the computation of interfacial position, frequencies, velocities, and accelerations but also every pinch-off event in time was identified.

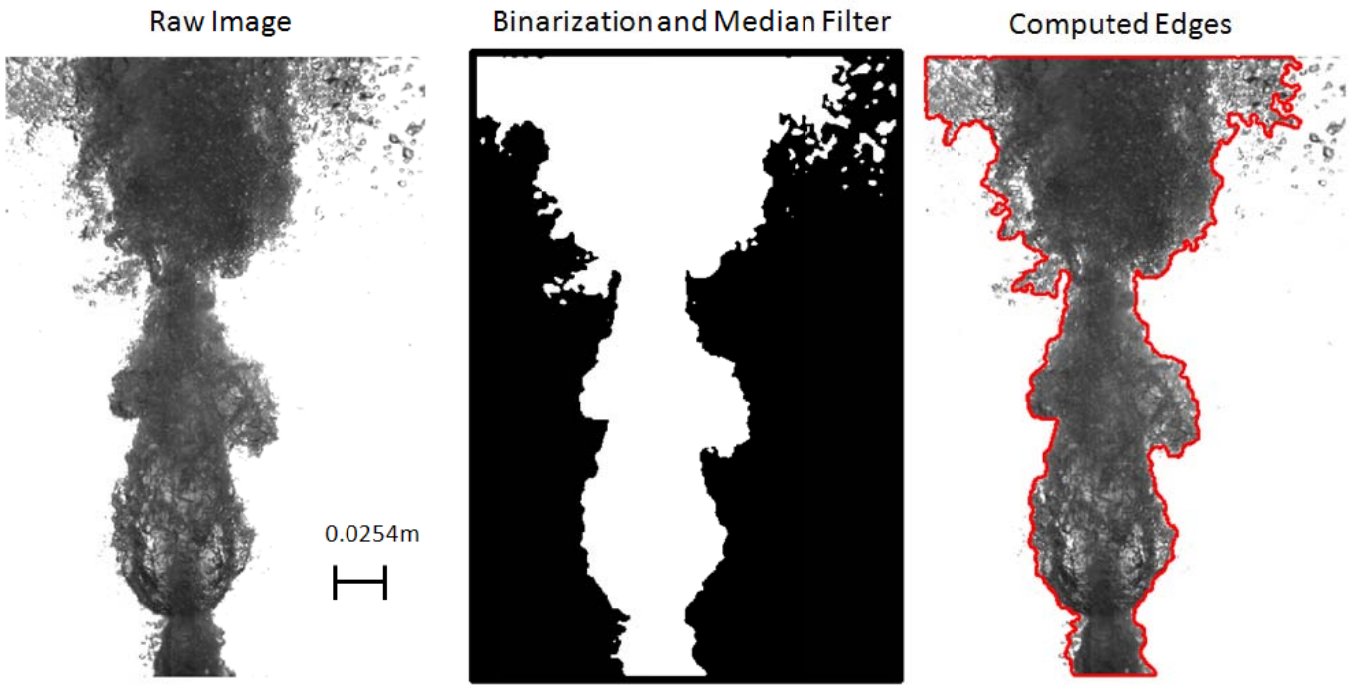

Figure 4. Steps used to detect the jet boundary. The process neglects outliers such as bubbles torn from the interface to accuracy track the phase boundary.

RESULTS AND DISCUSSION

In this paper we employ photographic measurements to quantify the effects of Mach number and aspect ratio (AR) on A) the spatial distribution of gas jet pinch-off, B) the penetration of submerged gas jets in water, and C) interfacial unsteadiness.

Analysis of the Jet Pinch-Off

One of the goals of this research was to quantify the effect of jet aspect ratio and Mach number on the jet pinch-off distribution. The phenomenon of pinch-off is largely due to the large density variation between the gas jet and the ambient waters. At some downstream position the gas jet can no longer support the local hydrostatic pressure and the gas jet will pinch-off. At this downstream location the flow is driven by buoyancy as opposed to momentum. Using the high speed photography and analysis methods presented above the distribution of pinch-off locations is quantified herein.

The number of pinch-off events for each aspect ratio and Mach number is shown in Figure 5. In several test cases no pinch-off events were observed namely AR 10 Mach 1.5 and AR 20 Mach 1.3 and 1.5. The number of pinch-off events is scaled by the total viewing length available divided by the length of the nozzle (l), which for a rectangular nozzle is also the geometric length scale L_Q [21]. This geometric length scales the jet development in single phase (i.e. gas jet in ambient gas environment) jets. A shown in Figure 5 the number of pinch-off events has a logarithmic decay with increasing Mach number and when appropriately scaled appears to be somewhat constant across all aspect ratio nozzles. These results indicate that increasing Mach number decreases the likelihood of a pinch-off event as Mach number is increased.

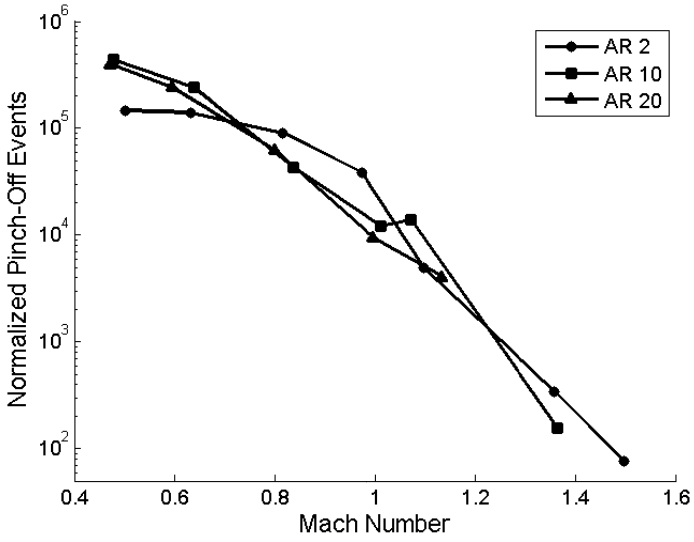

Figure 5. The number of pinch-off events observed for each Mach number and aspect ratio. The number of pinch-off events was normalized by the total observation distance divided by the width of the nozzle.

The spatial distribution of pinch-off events was experimentally observed to be dependent on the aspect ratio of the injector. An example of this is shown in Figure 6 for the AR 10 nozzle which shows a peak in the number of pinch-off events at $y/L_Q \approx$ 3-5. The subsonic Mach numbers 0.5, 0.6, and 0.8 show a broader range of pinch-off locations ranging from $y/L_Q \approx$ 3-9 while the sonic and supersonic jets typically show peaks of smaller width.

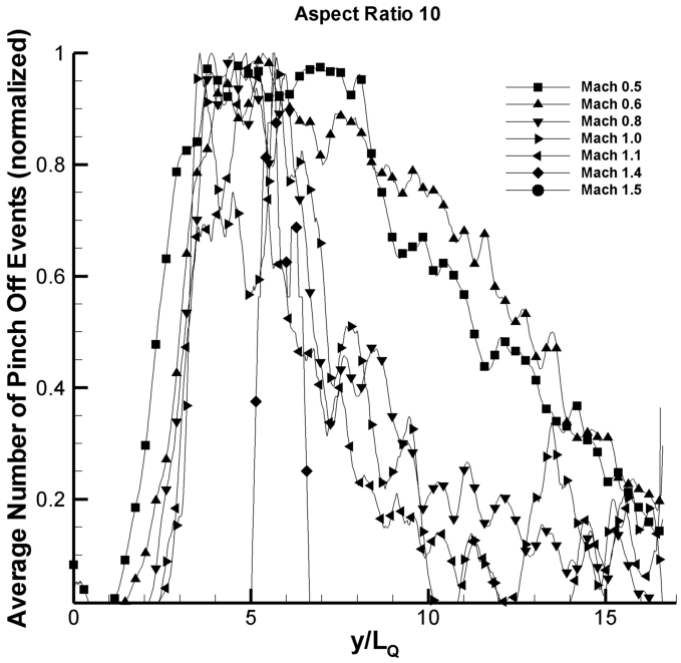

Figure 6. Spatial distribution of pinch-off events for AR 10. For all Mach numbers except Mach 1.5 the jets have a maximum in pinch-off events at $y/L_Q \approx$ 3-5. The Mach 1.5 jet did not pinch-off.

The axial location of maximum pinch-off events for all aspect ratio nozzles and Mach numbers is shown in Figure 7. Values of zero indicate the jet did not pinch-off, namely AR 10 Mach 1.5 and AR 20 Mach numbers 1.3 and 1.5. The AR 2 nozzles show a remarkable dependence on Mach number with subsonic Mach numbers having peaks between $y/L_Q \approx$ 23-26 while sonic and supersonic Mach numbers have peaks over the range $y/L_Q \approx$ 11-14. The latter range of values corresponds to the experimentally observed location of maximum streamwise turbulence levels in round gas jets [[22]; [21]]. The AR 10 and 20 nozzles show no dependence on Mach number with the maximum number of pinch-off events observed over the interval $y/L_Q \approx$ 3-5.

The variance in pinch-off location with aspect ratio suggests that aspect ratio plays a fundamental role in the development of rectangular jets. Quinn [23] showed through measurements of AR 2, 10, and 20 single phase gas jets that the streamwise turbulence fluctuations reach a maximum near $y/L_Q \approx$ 10-15 for the AR 2 nozzle and $y/L_Q \approx$ 5 for the AR 10 and 20 nozzles. These results are remarkably similar to those shown here and it is possible that the streamwise turbulence levels act as a perturbing factor on the interface, being directly responsible for pinch-off. Additionally, the axial position of $y/L_Q \approx$ 3 [16] and $y/L_Q \approx$ 5 [24] were shown to correspond to the axial position of "axis switching," where the jet cross section increases significantly in the nozzle width dimension. This point corresponds to the departure of the jet from two-dimensional to axisymmetric flow behavior, and the tendency of rectangular gas jets to switch major axes during evolution suggests this point to be a prime location for pinch-off to occur.

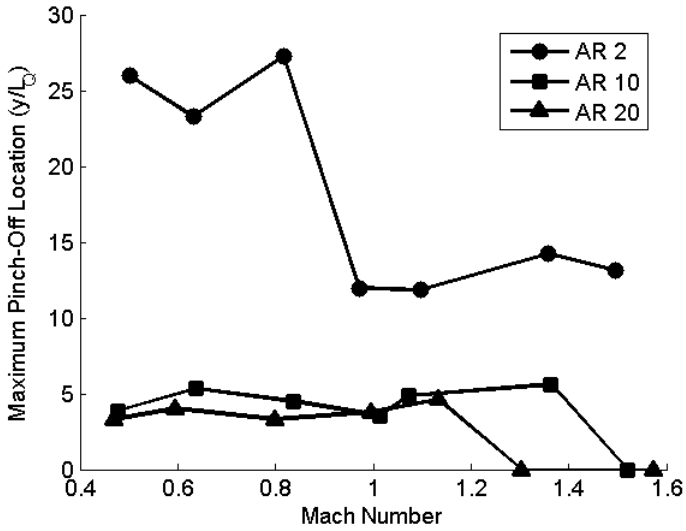

Figure 7. The axial position having the most pinch-off events is dependent on the aspect ratio of the nozzle. Tests for nozzles AR 10 Mach 1.5 and AR 20 Mach numbers 1.3 and 1.5 showed no pinch-off events over the measured domain.

Jet Penetration Distance

The length of gas jet penetration into the ambient waters is governed by the Mach number and aspect ratio. The jet penetration distance is defined as the maximum length along the jet centerline the gas jet maintains a presence over the test sample for 98.5% of the measured time. The penetration distance must be described statistically as submerged gas jets naturally pulsate and the penetration distance varies in time. Several previous works have measured the penetration distance of submerged round gas jets using electroresistive or optical probes lowered into the water and traversed through space [[25], [26], and [27]]. Ozawa and Mori [26] use this method to determine what they call gas holdup, which is a statistical mapping of how far gas penetrates into the surrounding waters. If water was present at the measurement point an electrical circuit was completed and registered a value of 1 and if gas was present a value of 0 was recorded. By summing up all of these values in time for many points in space the time fraction of gas penetration at that point was calculated. Here we implement a similar approach but instead we use our non-invasive imaging that measures the position of the gas jet spatially at each instant of time. From the binarized images, as shown in Figure 4, we sum the values of each pixel over time and divide by the measurement duration to arrive at a time fraction of gas

presence for all pixel locations as shown in Figure 8 where the color contour indicates the percentage of time that a certain location in the field of view was occupied by gas. A comparison of the Mach 0.4 and Mach 0.9 jets show obvious differences, especially in the length of a gaseous core which occupies a volume for a large percentage of the test record.

One advantage of this approach is that it enables distinguishing between bubbles that have fractured from the gas jet column and an orifice attached continuous jet, which is not possible using the electroresistive probe. We determine the length of the gas jet penetration only for orifice-attached gas jets, meaning that our calculations ignore any portion of the gas jet that has ruptured and is rising to the surface as an independent bubble.

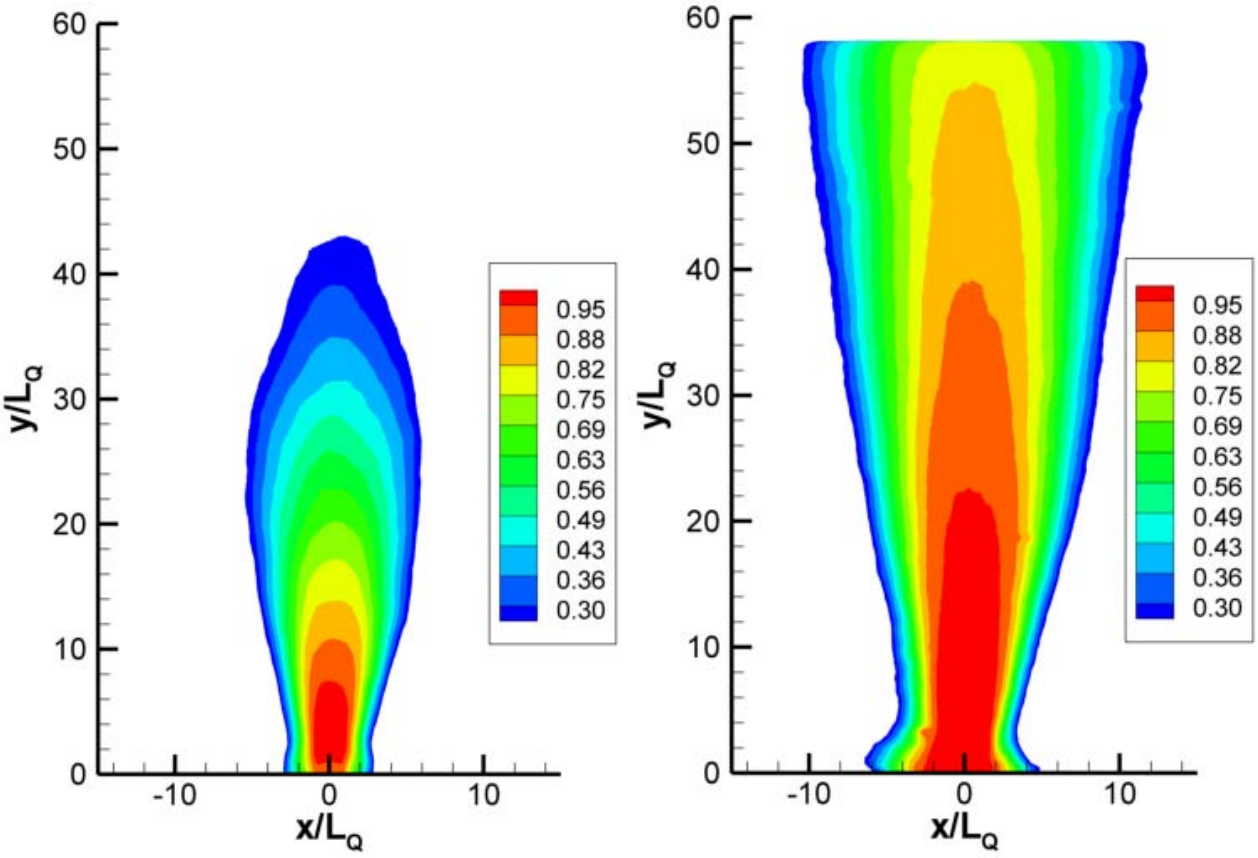

Figure 8. Gas holdup contours for a AR 2 Mach 0.4 jet (left) and Mach 1.0 jet (right). The sonic gas jet penetrates further into the quiescent fluid statistically than the subsonic gas jet.

The jet penetration distance for all aspect ratio nozzles is shown in Figure 9 as a function of Mach number. Cases for which the jet penetration was greater than the sampled viewing area are shown as disconnected points. In general, increasing aspect ratio and increasing Mach number yields greater penetration distances. The bubbling to jetting transition point is the sonic point as a large jump in penetration length occurs at or after this Mach number. The jet penetration increases non-linearly in the supersonic regime, with at least the AR 2 nozzle having a trend indicative of a cubic relationship such as $y_P \approx C(M - 1)^{1/3}$, where y_P is the jet penetration distance, C is a constant dependent on aspect ratio, and M is the injection Mach number. The fact that the inflection point occurs at the sonic point is further proof that the transition from bubbling to jetting occurs at the sonic point in rectangular jets. The sonic point is taken as the bubbling to jetting transition point in round submerged gas jets as well [[28]; [1]], indicating a fundamental change in the jet dynamics after this point.

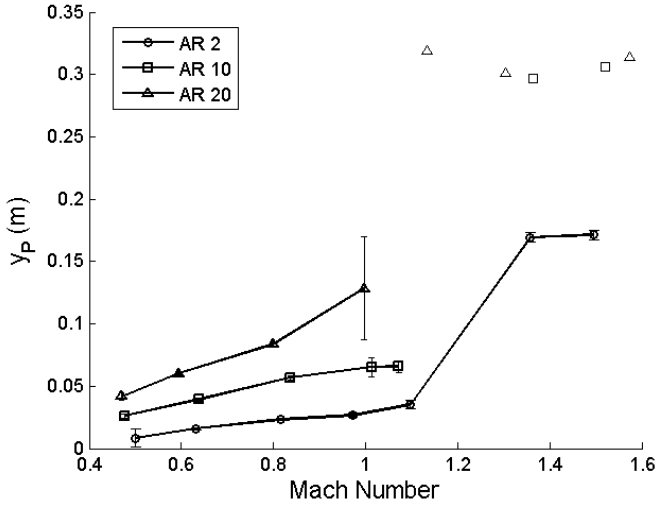

Figure 9. The jet penetration distance increases with increasing aspect ratio and Mach number. The unconnected data points correspond to cases in which the jet penetration distance was greater than the field of view; the jet penetrated at least this distance.

In light of the nearly linear jet penetration distance with Mach number in the subsonic and sonic regimes it is anticipated that some scaling relationship exists between the different aspect ratio jet penetration distances. As shown in the left plot of Figure 10 the jet penetration in physical units increases with the power law relationship $y_P = 1.95\dot{m}^{0.74}$ which gives a coefficient of determination of 0.93.

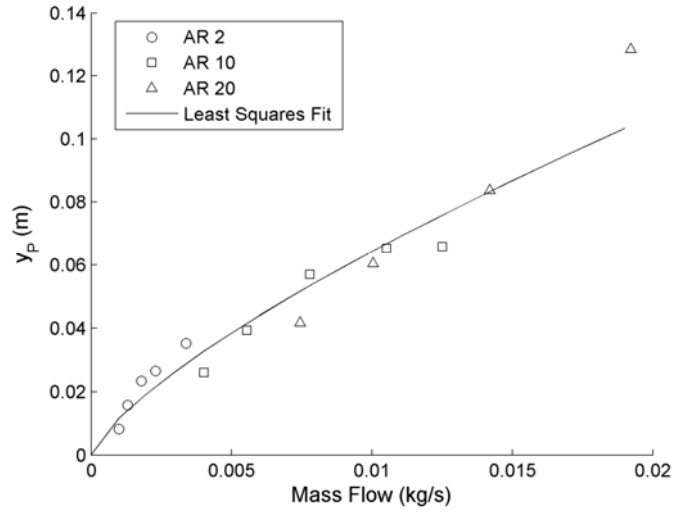

Figure 10. Two aspects of the jet penetration across all aspect ratio nuzzles tested. Left plot shows, in physical units, the jet penetration distance increases with mass flow according to a power law relationship. Right plot shows, in nondimensional units, the jet penetration increases linearly.

The nondimensional jet penetration distance is shown in the left plot of Figure 11 and is scaled by the developmental length L_Q. For rectangular nozzles this length is simply the long dimension of the nozzle (l). The AR 10 and 20 nozzle curves collapse reasonably well using L_Q to scale the jet penetration length. The AR 2 curve does not scale similarly. This may be a manifestation of the fact that the AR 2 nozzle is nearly axisymmetric after a smaller development length than the AR 10 and 20 nozzles. The effects of aspect ratio on rectangular jet development have been well documented. Krothapalli et al [14] has reported the effects of aspect ratio on the development of single phase rectangular jets and note that the downstream distance where the velocity profile follows similarity seems to depend on aspect ratio, mainly due to merging of the shear layers located in the plane of the long nozzle dimension. Using hot-wire anemometer measurements Sfeir [16] confirmed the importance of aspect ratio on velocity decay and showed the departure from two-dimensional effects which are influenced by the nozzle aspect ratio. Thus, both the AR 10 and 20 nozzles are less axisymmetric near the nozzle and require a larger development length to reach the axisymmetric zone where all memory of the original rectangular configuration is lost [12].

Figure 11 shows the jet penetration distance scaled by the development length scale and the curves collapse reasonably well with a nearly linear trend, with the exception of the AR 2 nozzle. This discrepancy in the penetration distance between the AR 2 and the AR 10 and 20 nozzles is attributed to the differences in the jets, as the AR 2 is nearly axisymmetric and the others are far from axisymmetric. In terms of jet penetration efficiency, the AR 2 nozzle performs best.

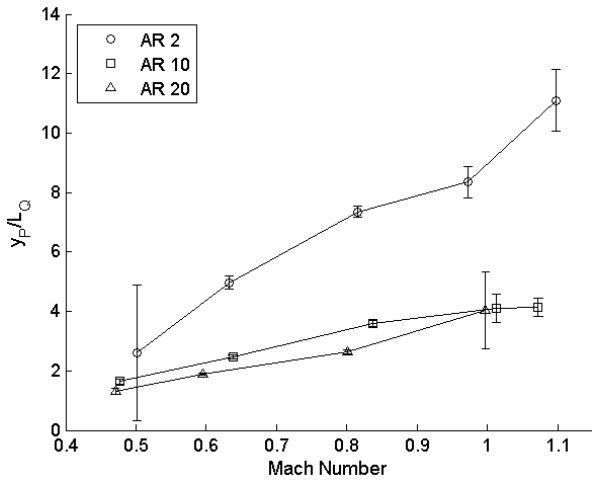

Figure 11. The jet penetration distance is scaled by L_Q. The AR 10 and 20 jet penetration curves follow similar trends while the AR 2 does not.

The jet spreading rate, which is indicative of mixing and entrainment at the interface, was found to be a function of both Mach number and aspect ratio as shown in Figure 12. In general, increasing aspect ratio and Mach number increase the spreading rate. The trend of increasing jet spreading angle with

increasing aspect ratio has been noted in a number of studies of single phase rectangular [[23]; [18]; [13]] and planar [7] jets. Zaman [3] measured the entrainment on Mach 0.95 jets of aspect ratio 2-38 and found that entrainment rates increased significantly only for AR ≥ 10. In our data, this trend is also observed. Prior to Mach 1.35 both the AR 2 and AR 10 have about the same spreading rates, while the AR 20 jet has a much greater spreading rate. The similarity in jet spreading for the AR 2 and 10 nozzles suggests the entrainment rate mechanisms may be similar.

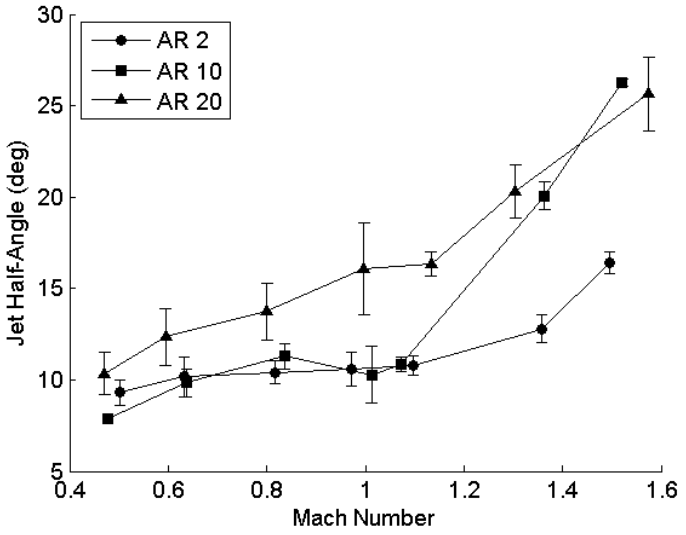

Figure 12. The average jet spreading angle is a function of both aspect ratio and Mach number. Generally, the spreading angle is greater for supersonic flows and higher AR nozzles.

It is fairly intuitive that increasing the aspect ratio moves the jet away from a near-axisymmetric case (AR 2) into a fully three-dimensional case. The sharp gradients at the corners of a large aspect ratio jet are quickly smeared due to instabilities which tend to enhance mixing [15]. The effect of Mach number on the spreading rate is less clear. It is interesting to note in Figure 12 the effect of Mach number on the AR 10 nozzle. After maintaining a slowly increasing spreading angle throughout the subsonic and transonic domain the spreading angle quickly increases near Mach 1.35. After this point the spreading rate becomes similar to values obtained for the AR 20 nozzle. This is in contrast to the AR 20 nozzle, which shows a strongly increasing jet spreading rate as Mach number is increased.

Based on these results, it is hypothesized that the interfaces generated by submerged rectangular gas jets are primarily influenced by instabilities whose relative strength is dependent on the aspect ratio. Stability may be directly linked to entrainment, as interfacial wave production and subsequent collapse leads to entrainment of ambient fluid into the jet, and therefore exerts a strong influence on the jet spreading rate. Mach number plays a secondary role and as seen in Figure 12 is apparently a triggering mechanism which can take a nominally stable jet, such as seen in the subsonic AR 10 nozzle with a jet spreading rate similar to the subsonic AR 2 nozzle, and rapidly increase the jet spreading rate. After the transonic regime the AR 10 spreading ratio increases drastically and is comparable to the AR 20 spreading rate. Although the AR 2 nozzle also shows an increase in the jet spreading past Mach 1.1 it does not increase to the extent seen in the AR 10 and 20 nozzles. In other words, cases AR 2 and 20 correspond to mostly stable and unstable jetting behavior in the subsonic and sonic regimes with AR 10 corresponding to a nominally stable jet until appropriately perturbed. This perturbation could come in the form of compressibility effects, such as shock-cell structures [6] or screech feedback mechanisms [[3]; [29]].

Unsteady Interfacial Characteristics

The interfacial unsteadiness was directly computed by taking the average deviation (AD) of the interface position and the results are shown in Figure 13-Figure 15 for the AR 2-10 nozzles, respectively. All dimensions are normalized by width (w) of the rectangular nozzle. With the exception of the AR 20 Mach 0.5 test supersonic nozzles generated the most unsteadiness near the nozzle and the least downstream of y/w ~ 10 – 12. The correspondence of this switch in interfacial behavior after y/w ~ 10 – 12 interface unsteadiness suggests that the shear layers emanating from the width of the nozzle plays a large role in governing the jet development by directly contributing to the stability of the interface. The magnitude of the interfacial movement increases with increasing aspect ratio as well. In general, increasing Mach number is seen to have a stabilizing effect on the interface with supersonic gas jets having less interfacial motion than subsonic jets.

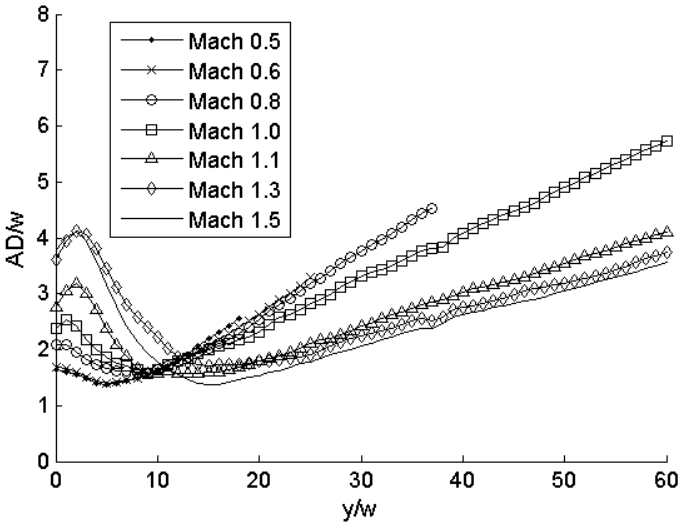

Figure 13. Average deviation of interface for AR 2 nozzle.

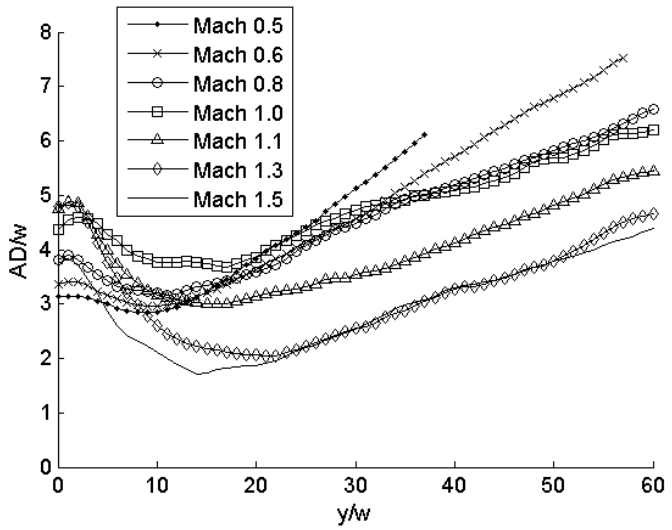

Figure 14. Average deviation of interface for AR 10 nozzle.

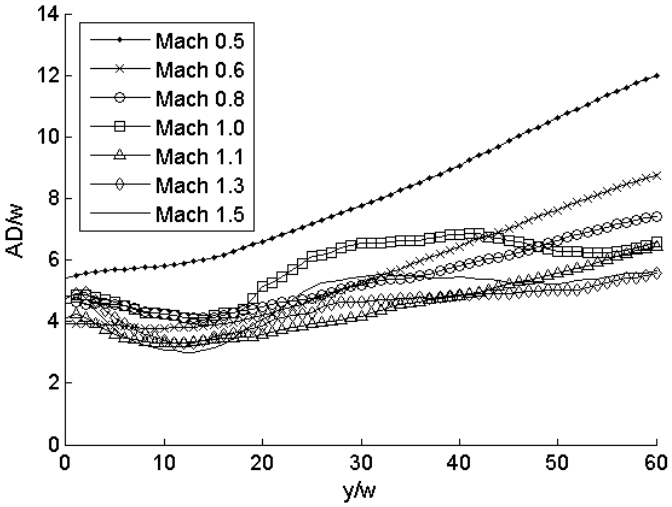

Figure 15. Average deviation of interface for AR 20 nozzle.

Although stability and the unsteady interface motions reported here are fundamentally different they are phenomenology similar. This is apparent from the results reported as increased interfacial motions are experimentally correlated to a less stable jet exhibiting a greater number of pinch-off events (consider Figure 5). Thus, the growth of the interface unsteadiness as it evolves downstream of the orifice may be linked to the spatial growth rate of the interface unsteadiness. This is plotted for all Mach numbers and aspect ratios in Figure 16. The scale is nondimensional and was computed from the slope of the line which best fits the data shown in Figure 13-Figure 15. The line is fitted after approximately y/w ~ 12 to ensure the jet is fully developed. The characteristics of the AR 2 nozzle is qualitatively similar to the results of Chen and Richter [30], as the spatial growth rate increases to a maximum in the sonic region and then rapidly decreases in the supersonic regime. The AR 10 and 20 cases follow a separate trend, having decreasing spatial growth rates until the sonic point and increasing growth rates in the supersonic regime. A manifestation of the increased growth rate in the supersonic regime for the AR 10 and 20 nozzles is also seen in Figure 12 as in the supersonic regime these nozzles had much greater spreading angles, and thus entrainment of local fluid. These results are interesting in that the AR 2 case corresponds to a nearly axisymmetric gas injection case whereas the AR 10 and 20 are fully three-dimensional by virtue of their large aspect ratios. This difference in growth rate as a function of aspect ratio suggests a different instability mechanism which governs rectangular, as opposed to circular, submerged gas jets. While several analytical studies have been conducted on submerged round gas jet stability [[30]; [31]; [32]], there are no studies known to the authors which analytically explore the interfacial stability of rectangular gas injection in water. Future research should pursue an analytical approach to yield insight into this problem.

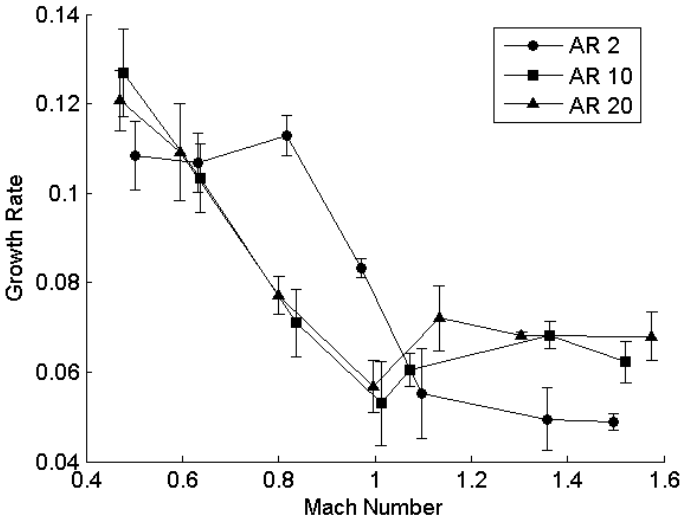

Figure 16. Spatial growth rate for all aspect ratio nozzles. The growth rate is a nondimensional scale representing the rate of interface unsteadiness downstream and is given by the slope of the best fit line passing through the AD points.

CONCLUSIONS

Gas jets formed by rectangular nozzles submerged in water were studied using a non-invasive photographic technique which allowed simultaneous measurements of the entire interface. Three aspect ratios were studied corresponding to 2, 10, and 20 with all nozzles sharing a common width. As far as the authors know this study represents the first time the effects of aspect ratio on a submerged gas jet have been studied. The main conclusions of this work are:

Buoyant jets were observed to consistently pinch-off at a spatial location corresponding to the maximum axial velocity turbulence fluctuations when normalized by the length scale L_Q. The number of pinch-off events decreases in a logarithmic fashion with increasing Mach number.

The jet penetration increases linearly for all aspect ratio nozzles in the subsonic and transonic regimes. After this point the jet penetration distance increases in a nonlinear fashion. The AR 2 nozzle showed a jet penetration trend of $y_P \approx C(M - 1)^{1/3}$, but the penetration of the supersonic AR 10 and 20 test cases was so great that this distance was not measureable.

The jet spreading rate, which is indicative of entrainment, shows dependence on both aspect ratio and Mach number. The AR 2 and 10 nozzles show similar spreading rates until the transonic regime, after which point both increase. However, the AR 20 nozzle has a much greater spreading rate regardless of Mach number. The AR 10 spreading rate increased to the level of the AR 20 nozzle in the supersonic regime, indicating the AR 10 nozzle sustained a significant change in its interfacial behavior as it became supersonic. The mechanism for the switch in behavior for the AR 10 nozzle in the supersonic regime is not clear.

The jet unsteadiness near the orifice is a function of the Mach number and aspect ratio. In general increasing Mach number decreases unsteadiness and increasing aspect ratio increases unsteadiness. All nozzles showed a switch in interfacial unsteadiness after $y/w \sim 10 - 12$, with supersonic jets be the least stable prior to this point and the most stable after this point.

The increase in interface unsteadiness downstream was computed and is indicative of the spatial instability growth rate. The results indicate that the AR 2 nozzle follows a trend similar to that predicted by Chen and Richter [30] while the AR 10 and 20 nozzles follow a separate trend. This suggests a fundamentally different mechanism for interfacial stability in rectangular jets as opposed to round jets.

ACKNOWLEDGEMENTS

This research was sponsored by the Naval Surface Warfare Center, Dahlgren Division. Mr. John Busic and Dr. Jon Yagla served as the technical monitors. Their support is gratefully acknowledged.

REFERENCES

[1] Mori, K., Ozawa, Y., and Sano, M., 1982, "Characterization of Gas-Jet Behavior at a Submerged Orifice in Liquid-Metal," Transactions of the Iron and Steel Institute of Japan, 22(5), pp. 377-384.

[2] Sano, M., Makino, H., Ozawa, Y., and Mori, K., 1986, "Behavior of Gas-Jet and Plume in Liquid-Metal," Transactions of the Iron and Steel Institute of Japan, 26(4), pp. 298-304.

[3] Zaman, K. B. M. Q., 1999, "Spreading Characteristics of Compressible Jets from Nozzles of Various Geometry," Journal of Fluid Mechanics, 383(pp. 31.

[4] Loth, E., and Faeth, G. M., 1989, "Structure of Underexpanded Round Air Jets Submerged in Water," International Journal of Multiphase Flow, 15(4), pp. 589-603.

[5] Zhao, Y. F., and Irons, G. A., 1990, "The Breakup of Bubbles into Jets During Submerged Gas Injection," Metallurgical Transactions B-Process Metallurgy, 21(6), pp. 997-1003.

[6] Loth, E., and Faeth, G. M., 1990, "Structure of Plane Underexpanded Air Jets into Water," AIChE Journal, 36(6), pp. 818-826.

[7] Deo, R. C., Mi, J., and Nathan, G. J., 2007, "The Influence of Nozzle Aspect Ratio on Plane Jets," Experimental Thermal and Fluid Science, 31(8), pp. 825-838.

[8] Gutmark, E., and Wygnanski, I., 1976, "The Planar Turbulent Jet," Journal of Fluid Mechanics, 73(pp. 30.

[9] Antonia, R., Browne, L., Rajagopalan, S., and Chambers, A., 1983, "On the Organized Motion of a Turbulent Plane Jet," Journal of Fluid Mechanics, 134(pp. 17.

[10] Gordeyev, S. V., and Thomas, F. O., 1999, "Temporal Subharmonic Amplitude and Phase Behaviour in a Jet Shear Layer: Wavelet Analysis and Hamiltonian Formulation," Journal of Fluid Mechanics, 394(-1), pp. 205-240.

[11] Gordeyev, S. V., and Thomas, F. O., 2000, "Coherent Structure in the Turbulent Planar Jet. Part 1. Extraction of Proper Orthogonal Decomposition Eigenmodes and Their Self-Similarity," Journal of Fluid Mechanics, 414(-1), pp. 145-194.

[12] Sforza, P., Steiger, M., and Trentacoste, N., 1966, "Studies on Three-Dimensional Viscous Jets," AIAA Journal, 4(5), pp. 6.

[13] Lozanova, M., and Stankov, P., 1998, "Experimental Investigation on the Similarity of a 3d Rectangular Turbulent Jet," Experiments in Fluids, 24(5), pp. 470-478.

[14] Krothapalli, A., Baganoff, D., and Karamcheti, K., 1981, "On the Mixing of a Rectangular Jet," Journal of Fluid Mechanics Digital Archive, 107(-1), pp. 201-220.

[15] Tam, C., and Thies, A., 1993, "Instability of Rectangular Jets," Journal of Fluid Mechanics, 248(pp. 23.

[16] Sfeir, A., 1979, "Investigation of Three-Dimensional Turbulent Rectangular Jets," AIAA Journal, 17(10), pp. 5.

[17] Quinn, W., 1991, "Passive near-Field Mixing Enhancement in Rectangular Jet Flows," AIAA Journal, 29(4), pp. 4.

[18] Tsuchiya, Y., and Horikoshi, C., 1986, "On the Spread of Rectangular Jets," Experiments in Fluids, 4(4), pp. 197-204.

[19] Sahai, Y., and Guthrie, R. I. L., 1982, "Hydrodynamics of Gas Stirred Melts .1. Gas-Liquid Coupling," Metallurgical Transactions B-Process Metallurgy, 13(2), pp. 193-202.

[20] Dai, Z. Q., Wang, B. Y., Qi, L. X., and Shi, H. H., 2006, "Experimental Study on Hydrodynamic Behaviors of High-Speed Gas Jets in Still Water," Acta Mechanica Sinica, 22(5), pp. 443-448.

[21] Fischer, H., List, E., Koh, R., Imberger, J., and Brooks, N., 1979, *Mixing in Inland and Coastal Waters*, Academic Press, New York.

[22] Crow, S. C., and Champagne, F. H., 1971, "Orderly Structure in Jet Turbulence," Journal of Fluid Mechanics, 48(03), pp. 547-591.

[23] Quinn, W., 1992, "Turbulent Free Jet Flows Issuing from Sharp-Edged Rectangular Slots: The Influence of Slot Aspect Ratio," Experimental Thermal and Fluid Science, 5(pp. 12.

[24] Trentacoste, N., and Sforza, P., 1967, "Further Experimental Results for Three-Dimensional Free Jets," AIAA Journal, 5(5), pp. 6.

[25] Castillejos, A. H., and Brimacombe, J. K., 1987, "Measurement of Physical Characteristics of Bubbles in Gas-

Liquid Plumes .1. An Improved Electroresistivity Probe Technique," Metallurgical Transactions B-Process Metallurgy, 18(4), pp. 649-658.
[26] Ozawa, Y., and Mori, K., 1986, "Effect of Physical-Properties of Gas and Liquid on Bubbling Jetting Phenomena in Gas Injection into Liquid," Transactions of the Iron and Steel Institute of Japan, 26(4), pp. 291-297.
[27] Ito, K., Kobayashi, S., and Tokuda, M., 1991, "Mixing Characteristics of a Submerged Jet Measured Using an Isokinetic Sampling Probe," Metallurgical Transactions B-Process Metallurgy, 22(4), pp. 439-445.
[28] Mcnallan, M. J., and King, T. B., 1982, "Fluid-Dynamics of Vertical Submerged Gas Jets in Liquid-Metal Processing Systems," Metallurgical Transactions B-Process Metallurgy, 13(2), pp. 165-173.
[29] Zaman, K. B. M. Q., Dahl, M. D., Bencic, T. J., and Loh, C. Y., 2002, "Investigation of a 'Transonic Resonance' with Convergent Divergent Nozzles," Journal of Fluid Mechanics, 463(-1), pp. 313-343.
[30] Chen, K., and Richter, H. J., 1997, "Instability Analysis of the Transition from Bubbling to Jetting in a Gas Injected into a Liquid," International Journal of Multiphase Flow, 23(4), pp. 699-712.
[31] Chawla, T. C., 1975, "Kelvin-Helmholtz Instability of Gas-Liquid Interface of a Sonic Gas Jet Submerged in a Liquid," Journal of Fluid Mechanics, 67(FEB11), pp. 513-537.
[32] Subramaniam, K., Parthasarathy, R. N., and Chiang, K. M., 1999, "Three-Dimensional Temporal Instability of Compressible Gas Jets Injected in Liquids," Aiaa Journal, 37(2), pp. 202-207.